Supplementary Materials for

Enhancing Capacitive Deionization Performance of $NaMnO_2$ by Interlayer Engineering and Redox-reaction

Shiyong Wang [a], Gang Wang [b*], Xiaoping Che [a], Shuifei Wang [a], Chengxu Li [a], Duanzheng Li [a], Yunqi Zhang [a], Qiang Dong [c], Jieshan Qiu [a*]

[a] State Key Lab of Fine Chemicals, School of Chemical Engineering, Liaoning Key Lab for Energy Materials and Chemical Engineering, Dalian University of Technology, Dalian 116024, PR China

[b] School of Environment and Civil Engineering, Dongguan University of Technology, Dongguan 523106, Guangdong, PR China.

[c] School of Chemical Engineering and Technology, Xi'an Jiaotong University, Xi'an 710049, Shaanxi, PR China

1. Experimental Section

1.1 Synthesis of Colloidal MnO_2 Nanosheets

The colloidal MnO_2 Nanosheets were prepared by a previously reported with some modifications[1]. Briefly, 2.375 g of manganese nitrate was dissolved in 40 mL deionized water. Then, a mixture containing 6.9 mL of H_2O_2, 17.2 mL of tetramethylammonium hydroxide and 55.9 mL of deionized water was added into above solution under vigorous stirring. The mixture was stirred at room temperature overnight. The obtained suspension was dialyzed in deionized water for 48 h and further washed by using a centrifuge to remove the large precipitations.

1.2 Self-assembly preparation of $NaMnO_2$ and CNT/$NaMnO_2$ samples

Typically, 50 mL of deionized water containing 50 mg of $NaNO_3$ was added into 200 mL of the manganese oxide colloidal suspension (0.5 mg mL^{-1}) under vigorous stirring at 60 °C for 6 h. Then $NaMnO_2$ obtained was washed three times with water and then dried at 60 ℃ before measurements were performed. CNT/$NaMnO_2$ was also prepared through the same process as applied in the synthesis of $NaMnO_2$ except with adding 20 mg CNT.

1.3 Materials characterization

The morphologies and structures of the samples were characterized through field emission scanning electron microscopy (FE-SEM, FEI Sirion200) and transmission

* Corresponding author. E-mail: wghy1979@163.com (G Wang).
* Corresponding author. Tel: 0086-411-84986080. E-mail: jqiu@dlut.edu.cn (J.S. Qiu).

electron microscopy (TEM, JEM-2010F). The crystal structure and phase composition of the composites were investigated using powder X-ray diffraction (XRD, Bruker D8). Nitrogen adsorption–desorption isotherms were collected at 77 K by using an Autosorb 6B instrument to determine the texture properties of the samples. Thermogravimetric analysis (TGA) was performed with TG209 (NETZSCH Co.). XPS measurements were performed with an ESCALAB 250 (Thermo Scientific, USA) by using Al Kα (hν = 1486.6 eV) X-ray radiation. Inductively coupled plasma atomic emission spectroscopy (ICP-AES) was used to analyze the chemical composition of the $NaMnO_2$ samples and concentration of Mn in the tank after the cyclic test of AC//$NaMnO_2$.

1.4 Electrochemical Measurements

Cyclic voltammetry (CV), galvanostatic charge-discharge (GCD), and electrochemical impedance spectroscopy (EIS) were conducted by using a CHI 660E electrochemical workstation in 1 M NaCl solution. A three-electrode system consisting of a platinum foil as the counter electrode, an Ag/AgCl electrode (saturated KCl) as the reference electrode, and the sample was used as the working electrode. To prepare the working electrodes, a homogeneous slurry of sample, polytetrafluoroethene (PTFE), and carbon black with the mass ratio of 8:1:1 in ethanol was pressed by a rolling mill into a film and dried at 80 °C overnight. The obtained electrodes were pushed onto a titanium mesh which used as current collectors. The specific capacitance (C, F g^{-1}) was calculated from the CV curves as **Equation 1**:

$$C = \frac{\int I\,dt}{2 \times v \times \Delta V \times m} \quad \text{.....(1)}$$

Where *C* is the specific capacitance (F g^{-1}), *I* is the response current density(A), *v* is the potential scanning rate (V s^{-1}), *ΔV* is the voltage change (V), and *m* is the active material mass (g).

1.5 HCDI experiments

To prepare the membrane-free HCDI electrodes, 82.5 wt% active materials (AC, MnO_2, $NaMnO_2$ and CNT/$NaMnO_2$), 10 wt% carbon black, 6 wt% polyvinyl butyral (PVB), and 1.5 wt% polyvinylpyrrolidone (PVP) were mixed together to obtain a homogeneous slurry. Subsequently, the resulting slurry with about 100 mg of solids was cast on a graphite paper (5×7 cm^2) and then dried at 80 °C overnight. The thickness of AC, MnO_2, $NaMnO_2$ and CNT/$NaMnO_2$ are 120, 100, 100 and 100 μm, respectively. The HCDI cell consisting of an activated carbon (AC) electrode, a

$NaMnO_2$ electrode (or CNT/$NaMnO_2$) and a piece of anion exchange membrane (200 μm, Hangzhou Iontech Environmental Technology Co., Ltd. Zhejiang, China) was denoted as $NaMnO_2$//AC (or CNT/$NaMnO_2$//AC) (Figure S5), whereas that consisting of an AC electrode, a MnO_2 electrode and a piece of anion exchange membrane was denoted as MnO_2//AC. An ~1.5 mm thick silicon gasket and two pieces of ~120 μm thick nonwoven fabric were used as the spacer and separator of the HCDI cells, respectively. Different concentrations of NaCl and voltages were employed to investigate the desalination performance of the HCDI system in various operation conditions. Ion removal step was conducted by applying a voltage (0.4 V to 1.2 V) for a certain time, while the captured ions were released by applying negative voltage (-0.4 V to -1.2 V) for a certain time. A tank (2.5L) of NaCl aqueous solution with different concentrations (100 to 20000 mg L^{-1}, or 1.7 mM to 341.9 mM) was pumped into the CDI setup by a peristaltic pump at a flow rate of 9 mL min^{-1}, and then flowed into another tank. An electrochemical workstation (CHI 660E) was used to supply the needed voltage. The changes of effluent conductivity and pH were recorded by an ion conductivity meter and pH monitor systems. The NaCl solution concentration was calculated by a calibration curve according to the conductivity profiles. The ion removal capacity (IRC, Γ, mg g^{-1}), charge consumed (Σ, C g^{-1}) and charge efficiency (Λ) were defined as **Equation 2**, **Equation 3** and **Equation 4**, respectively:

$$\Gamma = \frac{\Phi \times \int (C_0 - C_t) \cdot dt}{m}$$

(2)

$$\Sigma = \frac{\int i \cdot dt}{m}$$

(3)

$$\Lambda = \frac{\Gamma \times F}{M \times \Sigma} \quad (4)$$

Where Φ is the flow rate (mL min^{-1}), C_0 and C_t are the influent and the effluent NaCl concentration (mg L^{-1}), respectively; m is the total mass of the two electrodes (g); i is the current during the adsorption process (A); F is the Faraday constant (96 485 C mol^{-1}); and M is the molar mass of NaCl (58.5 g mol^{-1}).

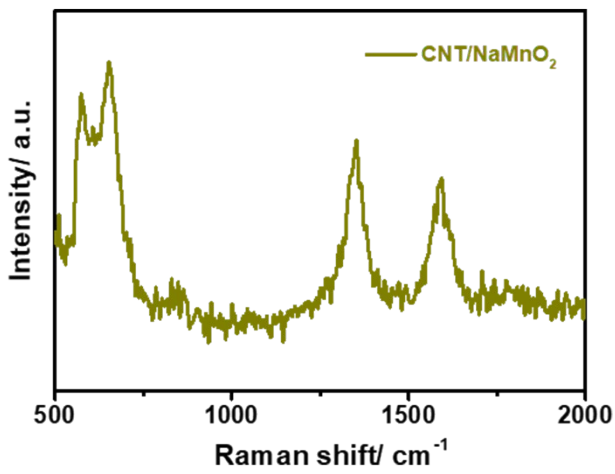

Figure S1 Raman spectra of the CNT/$NaMnO_2$.

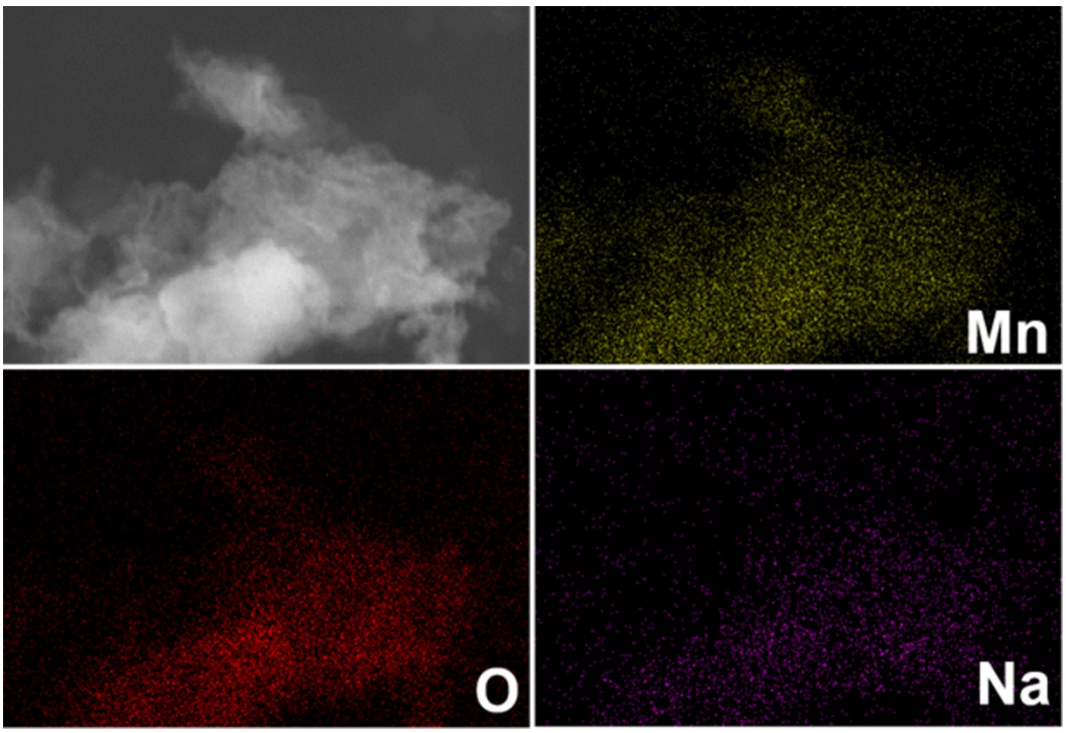

Figure S2 Elemental mapping of $NaMnO_2$.

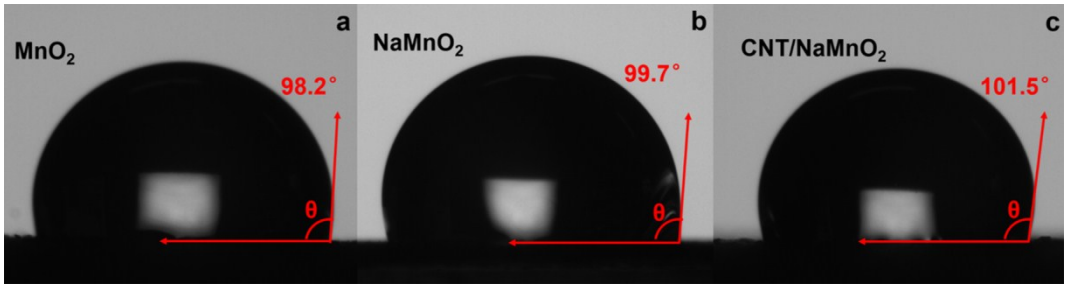

Figure S3 Water contact angle measurements of sampes

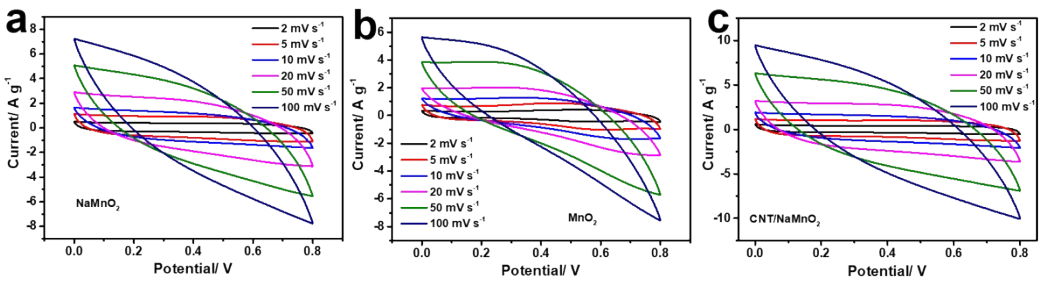

Figure S4 CV curves of (a) $NaMnO_2$, (b) MnO_2 and (c) CNT/$NaMnO_2$ at different scan rate.

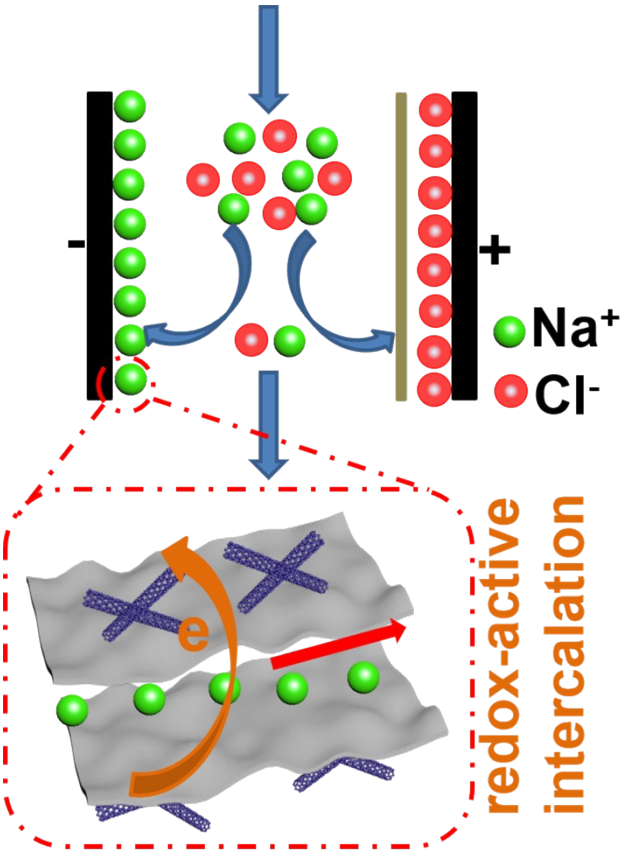

Figure S5 The schematic cell configuration of the HCDI consisting of the MnO_2-based and AC electrodes.

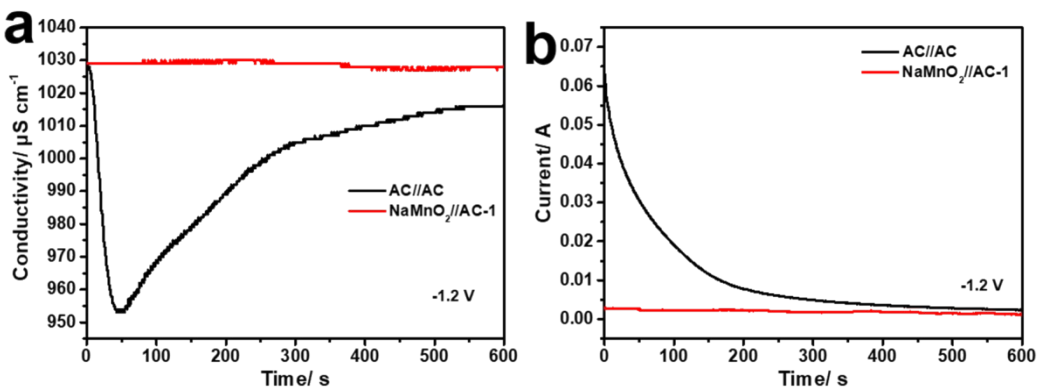

Figure S6 (a) conductivity (b) Current changes during the bias application with opposite polarity (-1.2 V)

A HCDI mode of $NaMnO_2$//AC-1 without anion exchange membrane was conducted at -1.2 V. As displayed in Figure S6, the $NaMnO_2$//AC-1 cell did not exhibit any reduction in concentration and current due to its operation principle depending on the polarity of bias, whereas the AC//AC cell showed the conductivity of effluent kept decreasing as same as when the applied voltage is +1.2 V.

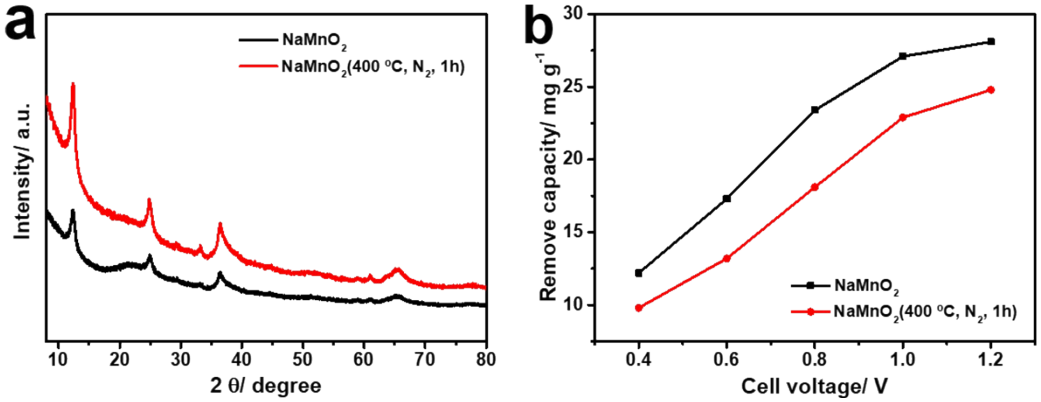

Figure S7 (a)XRD patterns and (b) IRC at various voltages of $NaMnO_2$ before and after thermal treatment.

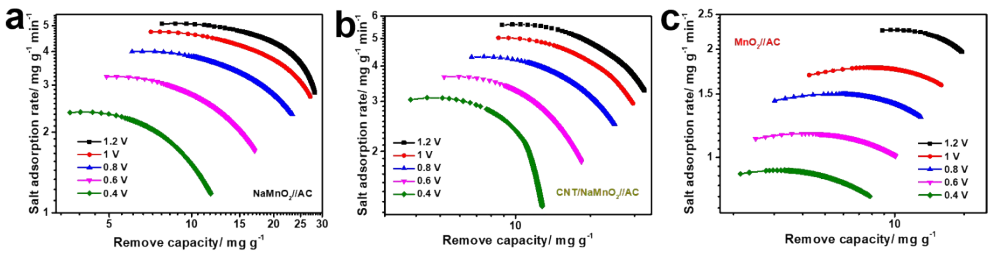

Figure S8 Kim-Yoon plots of (a) $NaMnO_2$//AC, (b) CNT/$NaMnO_2$ and (c) MnO_2//AC in NaCl solution with an initial concentration of 500 mg L^{-1} by varying the cell voltage.

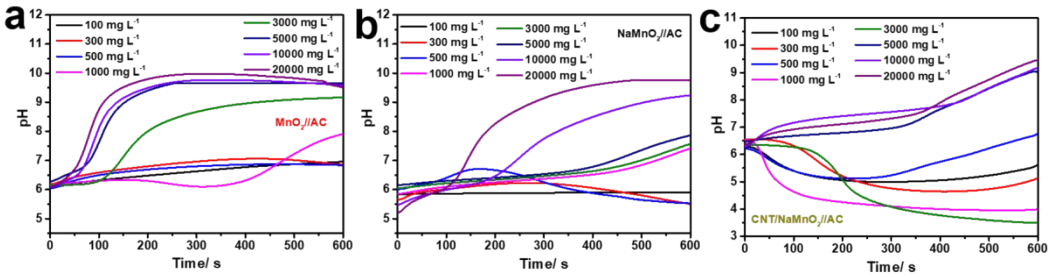

Figure S9 pH changes of the effluent during charge-discharge process when tested with 500 mg L^{-1} NaCl solution: (a) MnO_2//AC, (b) $NaMnO_2$//AC and (c) CNT/$NaMnO_2$//AC.

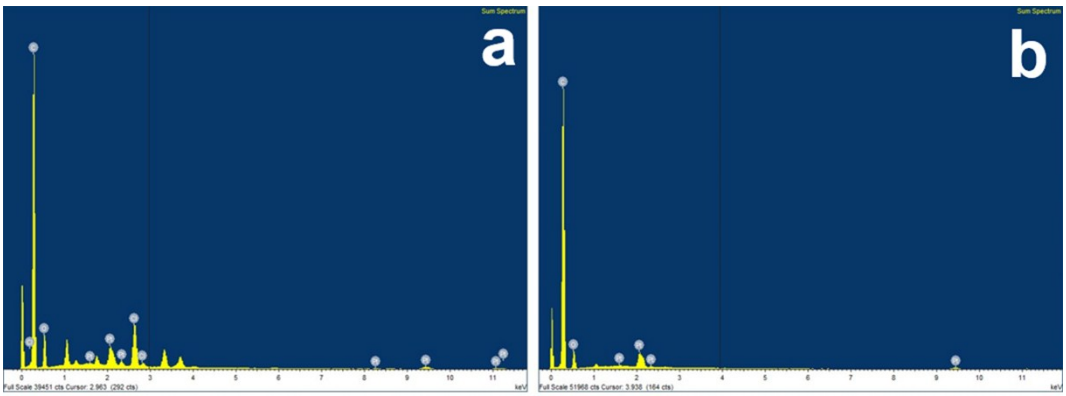

Figure S10 Representative EDS spectra of AC electrodes of $NaMnO_2$//AC after ion removal experiments.

EDS spectra are shown (a) before and (b) after washing of the electrode with copious amounts of deionized water, indicating Cl^- ions are physisorbed on the carbon surface.

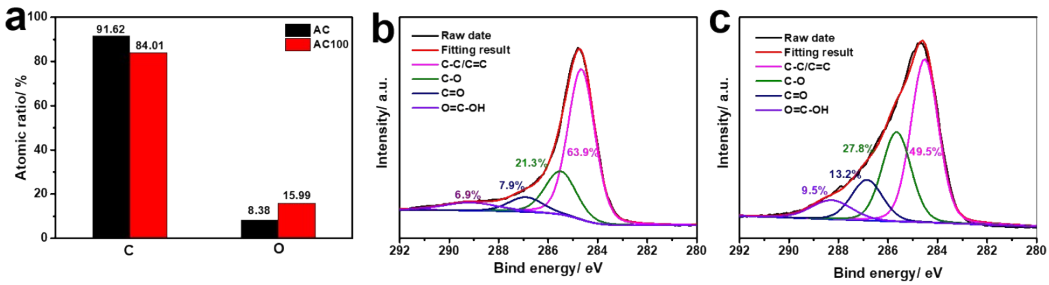

Figure S11 (a) atomic ratio of C, N, and O on the surface of AC after 100 cycles; (b) C1s XPS spectra of AC before cycles; (c) C1s XPS spectra of AC after 100 cycles.

Table S1 The compositions and the interlayer spacing of samples

	Chemical compositions measured by the ICP-AES method	Interlayer spacing (Å) calculated from the (001) peaks
$NaMnO_2$	$Na_{0.2}MnO_2$	7.17
$NaMnO_2$-IAS	$Na_{0.26}MnO_2$	7.21
$NaMnO_2$-IRS	$Na_{0.17}MnO_2$	7.15
CNT/$NaMnO_2$	CNT/$Na_{0.19}MnO_2$	7.18
CNT/$NaMnO_2$-IAS	CNT/$Na_{0.24}MnO_2$	7.22
CNT/$NaMnO_2$-IRS	CNT/$Na_{0.16}MnO_2$	7.16

Table S2 Comparison of desalination performance among different deionization systems

Materials	Cell configuration	voltage (V)	Exchange membranes	NaCl (mg L^{-1})	SAC (mg g^{-1})	Ion removal rate (mg g^{-1} min^{-1})	Reference
NC800-PEDOT	CDI	1.2	None	58.5	16.18	None	[2]
BNPC	CDI	1.4	None	500	16.63	2.1	[3]
GSSNA-11	CDI	1.2	None	500	22.09	1.6	[4]
rGO/Co_3O_4-A	HCDI	1.6	None	500	15.15	None	[5]
MnO_2/CNT−CS)	CDI	1.6	None	880	10.07	None	[6]
$Na_{0.44}MnO_2$//AC	HCDI	1.2	Anion	585	31.2	3.96	[7]
Na-birnessite//AC	HCDI	1.2	Anion and cation	878	31.5	None	[8]
α-MnO_2//AC	HCDI	1.2	Anion	880	22.1	6.66	[9]
$Na_4Ti_9O_{20}$//AC	HCDI	1.4	Anion	250	23.35	None	[10]
Birnessite δ-MnO_2//AC	HCDI	1	None	293	9.35	None	[11]
$NaMnO_2$//AC	HCDI	1.2	Anion	500	28.3	5.1	this work
CNT/$NaMnO_2$//AC	HCDI	1.2	Anion	500	32.7	5.7	this work
CNT/$NaMnO_2$//AC	HCDI	1.2	Anion	20000	42.6	7.3	this work

Reference

1. L. Ke, H. Ziyu, X. Zhonghua, M. Jizhen, S. Bin, Z. Jintao and M. Houyi, Cation Intercalation in Manganese Oxide Nanosheets: Effects on Lithium and Sodium Storage, *Angew. Chem. Int. Ed.,* 2016, **55**, 10448-10452.
2. Y. Li, J. Kim, J. Wang, N. L. Liu, Y. Bando, A. A. Alshehri, Y. Yamauchi, C. H. Hou and K. C. Wu, High performance capacitive deionization using modified ZIF-8-derived, N-doped porous carbon with improved conductivity, *Nanoscale*, 2018, **10**, 14852-14858.
3. Z. Wang, T. Yan, J. Fang, L. Shi and D. Zhang, Nitrogen-doped porous carbon derived from a bimetallic metal–organic framework as highly efficient electrodes for flow-through deionization capacitors, *J. Mater. Chem. A*, 2016, **4**, 10858-10868.
4. Z. U. Khan, T. Yan, L. Shi and D. Zhang, Improved capacitive deionization by using 3D intercalated graphene sheet–sphere nanocomposite architectures, *Environ. Sci.: Nano*, 2018, **5**, 980-991.
5. G. Divyapriya, K. K. Vijayakumar and I. Nambi, Development of a novel graphene/Co_3O_4 composite for hybrid capacitive deionization system, *Desalination*, 2019, **451**, 102-110.
6. Y.-H. Liu, T.-C. Yu, Y.-W. Chen and C.-H. Hou, Incorporating Manganese Dioxide in Carbon Nanotube–Chitosan as a Pseudocapacitive Composite Electrode for High-Performance Desalination, *ACS Sustainable Chem. Eng.*, 2017, **6**, 3196-3205.
7. J. Lee, S. Kim, C. Kim and J. Yoon, Hybrid capacitive deionization to enhance the desalination performance of capacitive techniques, *Energy Environ. Sci.*, 2014, **7**, 3683-3689.
8. B. W. Byles, B. Hayes-Oberst and E. Pomerantseva, Ion Removal Performance, Structural/Compositional Dynamics, and Electrochemical Stability of Layered Manganese Oxide Electrodes in Hybrid Capacitive Deionization, *ACS Appl Mater Interfaces*, 2018, **10**, 32313-32322.
9. B. W. Byles, D. A. Cullen, K. L. More and E. Pomerantseva, Tunnel structured manganese oxide nanowires as redox active electrodes for hybrid capacitive deionization, *Nano Energy*, 2018, **44**, 476-488.
10. F. Zhou, T. Gao, M. Luo and H. Li, Heterostructured graphene@$Na_4Ti_9O_{20}$ nanotubes for asymmetrical capacitive deionization with ultrahigh desalination capacity, *Chem. Eng. J.*, 2018, **343**, 8-15.
11. Z. Y. Leong and H. Y. Yang, A Study of MnO_2 with Different Crystalline Forms for Pseudocapacitive Desalination, *ACS Appl Mater Interfaces*, 2019, DOI: 10.1021/acsami.8b20880.